Journal of
Materials Chemistry A

Accepted Manuscript

This article can be cited before page numbers have been issued, to do this please use: J. Jiang, W. Liu, Y. Hou, H. Pan, W. Liu, D. Qi, K. Wang and X. Yao, *J. Mater. Chem. A*, 2018, DOI: 10.1039/C8TA00516H.

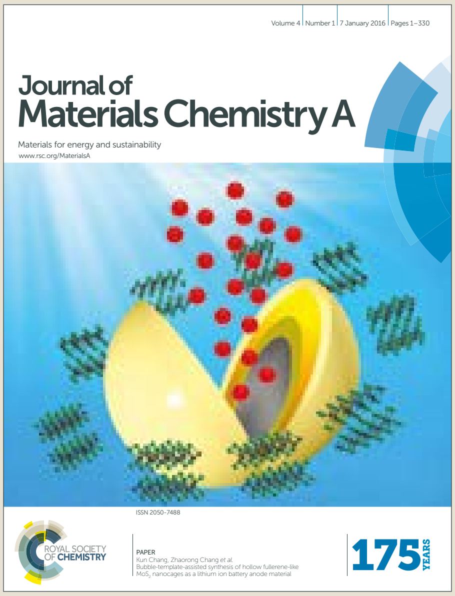

ROYAL SOCIETY
OF CHEMISTRY

rsc.li/materials-a

View Article Online
DOI: 10.1039/C8TA00516H

Journal Name

ARTICLE

Ethynyl-linked Fe/Co Heterometallic Phthalocyanine Conjugated Polymer for Oxygen Reduction Reaction†

Received 00th January 20xx,
Accepted 00th January 20xx

DOI: 10.1039/x0xx00000x

www.rsc.org/

Wenping Liu,[a] Yuxia Hou,[a,c] Houhe Pan,[a] Wenbo Liu,[a] Dongdong Qi,*[a] Kang Wang,*[a,b] Jianzhuang Jiang*[a] and Xiangdong Yao[b]

Sonagashira-Hagihara coupling reaction is utilized to fabricate the ethynyl-linked phthalocyanine (Pc) 2D conjugated polymers (CPs), affording the unprecedented heterometallic compound **$Fe_{0.5}Co_{0.5}$Pc-CP** and homometallic analogues **MPc-CP**s (M = Fe, Co) as comparisons. It is confirmed that the Fe and Co ions are well-defined/distributed with one metal ion encircled by four neighboring ions of the second metal in close proximity in the heterometallic conjugated polymer. Compared to homometallic analogues, the bimetallic polymer **$Fe_{0.5}Co_{0.5}$Pc-CP** is highly more efficient for oxygen reduction reaction (ORR), indicating that the interaction of Fe and Co ions may provide a synergistic effect on the activity. The ORR activity of **$Fe_{0.5}Co_{0.5}$Pc-CP** is with a similar ORR catalytic activity and superior stability to the commercial Pt/C in alkaline. Density functional theory calculation reveals that a fast 2 × $2e^-$ synergetic catalytic reaction pathway is essential for the excellent ORR in **$Fe_{0.5}Co_{0.5}$Pc-CP**.

Introduction

Oxygen reduction reaction (ORR) plays an important role in energy conversion and storage devices such as fuel cells and metal-air batteries.[1] Currently, noble metal platinum (Pt) is still the best catalyst for the ORR.[2] However, the high cost and scarcity, serious anode crossover, and methanol poisoning of Pt-based catalysts limit their large-scale commercial applications.[3] Non-precious high-performance alternatives towards ORR then become highly desired in this field, leading to the development of a wide range of non-Pt-based electrochemical catalysts including transition metal oxides,[4] carbon-based metal free materials,[5] and transition-metal-decorated carbon materials.[6] Among them, MN_x-based (M = Fe, Co) electrocatalysts have been extensively studied, which are among the most promising systems to replace expensive Pt based catalysts.[7,8] Notably, recent studies suggest that Fe&Co bimetallic MN_x-based materials have better catalytic activity compared to their single-element counterparts, as shown by PCN-FeCo/C,[8a] PANI-FeCo-C,[8b] (Fe,Co)/N-C,[8c] and FeCo-MFR/C.[8d] The higher catalytic activity of the bimetallic catalysts with both Fe and Co originates from the synergistic effect between the two metal centers, which should be closely related to the small spatial separation and ordered distribution of Fe and Co atoms. However, so far all the state-of-the-art $FeCoN_x$-based catalysts are fabricated through thermal treatment (typically 800-1000°C),[8] which is energy intensive and not environmentally friendly. Moreover, the high temperature thermal treatment makes it hard to approach the atomic-level ordering of the active components in the catalysts. This limits in-depth understanding the intrinsic reaction mechanism and further rational design of new $FeCoN_x$-based catalysts with improved catalytic performance.

Two dimensional (2D) organic conjugated polymers (CPs) are a novel class of polymeric materials with amorphous extended π-conjugated networks.[9] The high flexibility in the molecular design of components and the control of network structures for CPs makes them possessing well-defined structure and chemical composition. It is anticipated that simultaneous introduction of Fe- and Co-N_4-macrocyclic monomers with high ORR catalytic activity into the fabrication of the 2D CPs could achieve Fe&Co bimetallic MN_x-based catalysts with alternate distribution of Fe and Co fragments, which would provide an effective method towards creating high-performance ORR catalysts.

Herein, we developed a new $FeCoN_x$-based ORR electrocatalyst termed ethynyl-linked heterometallic phthalocyanine (Pc) conjugated polymer by means of Sonagashira-Hagihara coupling reaction between Fe[Pc(I)$_4$] and Co[Pc(ethynyl)$_4$] {[Pc(I)$_4$] = dianion of 2(3),9(10),16(17),23(24)-tetraiodophthalocyanine; [Pc(ethynyl)$_4$] = dianion of 2(3),9(10),16(17),23(24)-tetra(ethynyl)phthalocyanine}. The corresponding merits are summarized as follows: (1) Since Jasinski first reported a CoPc based electrocatalyst for a fuel cell cathode in 1964,[10] the ability of metallophthalocyanines to reduce molecular oxygen has been extensively studied.[11] It has

---

*a Beijing Key Laboratory for Science and Application of Functional Molecular and Crystalline Materials, Department of Chemistry, University of Science and Technology Beijing, Beijing 100083, China. *E-mail: jianzhuang@ustb.edu.cn, kangwang@ustb.edu.cn,qdd@ustb.edu.cn.*
b Queensland Micro- and Nanotechnology Centre, Griffith University, Nathan Campus QLD 4111, Australia.
c Department of Chemistry and Chemical Engineering, Henan Institute of Science and Technology, Xinxiang 453003, China.

† Electronic Supplementary Information (ESI) available: See DOI: 10.1039/x0xx00000x

View Article Online
DOI: 10.1039/C8TA00516H

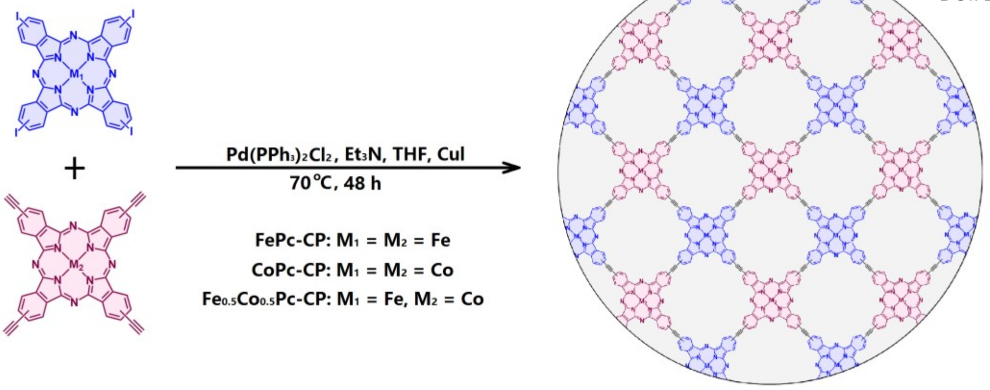

Scheme 1. Schematic diagram for the synthesis of the phthalocyanine conjugated polymers **MPc-CP**s (M = Fe, Co, and $Fe_{0.5}Co_{0.5}$).

been found that metallophthalocyanines, in particular iron and cobalt phthalocyanines, show good ORR activity but poor stability. Polymerization of metallophthalocyanines could significantly improve their physical and chemical robustness, possibly resulting in high stability. Moreover, the planar conjugated molecular structure makes the phthalocyanines as promising building blocks in the construction of 2D CP materials. (2) Sonagashira-Hagihara coupling reaction was employed to form carbon-carbon bonds between the terminal alkynes in Co[Pc(ethynyl)$_4$] and the aryl iodines in Fe[Pc(I)$_4$], which makes the well-arranged Pc units in the network with one chromophore originated from one starting Pc species encircled by four chromophores of the other Pc species. In addition, the coupling reaction was carried out under mild reaction conditions, circumventing high-temperature heat treatment and retaining the structures of Pc precursors in the catalyst materials. (3) The ethynyl-linked heterometallic Pc-based 2D conjugated polymer possesses well-defined chemical composition and alternate distribution of Fe and Co fragments, providing an ideal model for understanding the origin of the catalytic activity. Consequently, the derived heterometallic compound exhibits excellent ORR catalytic activity in alkaline media, which is comparable to commercial Pt/C, due to the synergetic effect between Fe and Co in this network.

Results and Discussion

Synthesis and characterization

For the purpose of fabricating the C≡C linked phthalocyanine 2D CPs *via* Sonagashira-Hagihara coupling reaction, corresponding metal free phthalocyanine monomers, namely 2(3),9(10),16(17),23(24)-tetraiodophthalocyanine {H_2[Pc(I)$_4$]} and 2(3),9(10),16(17),23(24)-tetra(ethynyl)phthalocyanine {H_2[Pc(ethynyl)$_4$]}, were prepared following the published procedures.[12] Metallization with Fe and Co afforded the phthalocyaninato metal complexes Fe[Pc(I)$_4$], Fe[Pc(ethynyl)$_4$], Co[Pc(I)$_4$], and Co[Pc(ethynyl)$_4$]. Sonagashira-Hagihara coupling between Fe[Pc(I)$_4$] and Co[Pc(ethynyl)$_4$] with a stoichiometric ratio of 1:1 in the mixed solvent of anhydrous THF:Et_3N (1:2) under the presence of bis(triphenylphosphine)palladium(II) chloride and CuI as catalysts at 70°C for 48 h provided the heteometallic Pc-based 2D conjugated network **$Fe_{0.5}Co_{0.5}$Pc-CP** as seen in Scheme 1. For comparative study, homometallic analogues **FePc-CP** (from the coupling of Fe[Pc(I)$_4$] with Fe[Pc(ethynyl)$_4$]) and **CoPc-CP** (from the coupling of Co[Pc(I)$_4$] with Co[Pc(ethynyl)$_4$]) were also fabricated. All these conjugated polymers are insoluble in water and organic solvents such as $CHCl_3$, CH_3OH, C_2H_5OH, N,N-dimethylformamide (DMF), tetrahydrofuran (THF), and acetone. Thermogravimetric analysis (TGA) indicated their good thermal stability with decomposition occurring over 350°C as shown in Fig. S1 (ESI†).

Fourier transform infrared (FT-IR) analysis confirms the successful fabrication of CPs from the two species of Pc monomers (Fig. 1a and S2 in ESI†). The absorptions contributed from the central aromatic Pc macrocycle including the wagging and torsion vibrations of C-H groups at 672-753 cm^{-1}, isoindole ring stretching vibrations at 1070-1420 cm^{-1}, and the C=N aza group stretching vibrations at 1584-1596 cm^{-1} in the IR spectra of the three **MPc-CP**s unambiguously demonstrate their Pc composition and structure.[13] The C-H stretching band at *ca.* 3289 cm^{-1} due to ethynyl groups of M[Pc(ethynyl)$_4$] and C-I vibration band at *ca.* 1033 cm^{-1} corresponding to the C-I groups of M[Pc(I)$_4$] get significantly attenuated in the IR spectra of the three **MPc-CPs**.[14,15] These results give a good evidence for the integration of these **MPc-CP**s from the coupling of M[Pc(I)$_4$] with M[Pc(ethynyl)$_4$] and in particular suggesting the well-arranged Pc units in the ethynyl-linked network with one chromophore originated from one starting Pc species encircled by four chromophores of the other Pc species as illustrated in Scheme 1. The solid-state UV-vis diffuse reflectance spectrum of **$Fe_{0.5}Co_{0.5}$Pc-CP** shows the phthalocyanine Soret band at 350-450 nm and Q-band at 600-800 nm, which are both slightly red-shifted compared to the corresponding phthalocyanine monomers, suggesting a highly conjugated nature of the polymer, Fig. 1b. This is also true for **CoPc-CP** and **FePc-CP** (Fig. S3 in ESI†). In addition, the newly prepared **MPc-CP**s were also characterized by solid-state ^{13}C CP/MAS NMR spectroscopy, showing one broad peak at 120-140 ppm assigned to the Pc macrocycle, (Fig. S4 in ESI†). Along with the change in the metal center from Co, to $Fe_{0.5}Co_{0.5}$, and Fe for the conjugated polymers, the signals due to the Pc

View Article Online
DOI: 10.1039/C8TA00516H

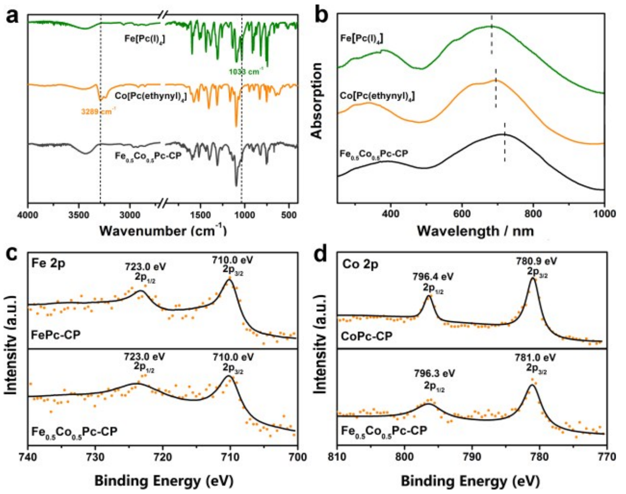

Fig. 1 (a) FT-IR spectra of **$Fe_{0.5}Co_{0.5}$Pc-CP** and corresponding phthalocyanine monomers in the region of 400-4000 cm^{-1}. (b) Solid-state UV-vis diffuse reflectance spectra of **$Fe_{0.5}Co_{0.5}$Pc-CP** and corresponding phthalocyanine monomers. XPS high resolution (c) Fe 2p and (d) Co 2p spectra of **CoPc-CP**, **FePc-CP**, and **$Fe_{0.5}Co_{0.5}$Pc-CP**.

macrocycle gradually downfield shift from 124 ppm for **CoPc-CP**, to 131 ppm for **$Fe_{0.5}Co_{0.5}$Pc-CP**, and 135 ppm for **FePc-CP**.

As shown in Fig. S5 (ESI†), the powder X-ray diffraction (PXRD) patterns gives no definite evident peaks, revealing the amorphous nature of these **MPc-CP**s, owing to the irreversible nature of the Sonagashira-Hagihara coupling reaction as well as the existence of less symmetrical isomers in M[Pc(I)$_4$]/M[Pc(ethynyl)$_4$]. Scanning electron microscopy (SEM) images show the morphology of the irregular agglomerated nanoparticles of these **MPc-CP**s, which consist of many pieces of nanosheets according to the transmission electron microscopy (TEM) images (Fig. S6 in ESI†), revealing the fabrication of the ethynyl-linked 2D network. The elemental-mapping images of the heterometallic **$Fe_{0.5}Co_{0.5}$Pc-CP** (Fig. S7 in ESI†), disclose the homogeneous distribution of the iron, cobalt, and nitrogen species throughout the whole network, suggesting the alternate distribution of Fe and Co fragments. This is also the same case for their homometallic analogues **FePc-CP** and **CoPc-CP**.

X-ray photoelectron spectroscopy (XPS) measurements were performed to analyze the surface composition and chemical valence state. As can be seen in the high-resolution Fe 2p XPS spectra in Fig. 1c, two peaks of the Fe $2p_{3/2}$ and Fe $2p_{1/2}$ were observed at 710.0 and 723.0 eV for **FePc-CP** and 710.1 and 723.0 eV for **$Fe_{0.5}Co_{0.5}$Pc-CP**, indicating the existence of Fe^{3+} in these two polymers.[16] The existence of Co^{2+} in **$Fe_{0.5}Co_{0.5}$Pc-CP** and **CoPc-CP** is confirmed by the two peaks of Co $2p_{3/2}$ and Co $2p_{1/2}$ observed at 781.0 and 796.3 eV for **$Fe_{0.5}Co_{0.5}$Pc-CP** and 780.9 and 796.4 eV for **CoPc-CP** in their high-resolution of Co 2p XPS spectra in Fig. 1d.[17] In the high-resolution N 1s spectra of **CoPc-CP**, **$Fe_{0.5}Co_{0.5}$Pc-CP**, and **FePc-CP**, the N 1s peak is deconvoluted into two sub-peaks at 399.3 and 398.7 eV, 399.3 and 398.7 eV, and 399.3 and 398.5 eV, respectively, corresponding to the metal coordinated pyrrole and aza nitrogen species (Fig. S8 in ESI†).[16,17] In addition, the peaks assigned to iodine and oxygen were also observed in the XPS overall spectra of the three CPs due to the residual iodine groups of M[Pc(I)$_4$] and axial coordinated OH^- or H_2O to the metal ions, respectively.

ORR electrocatalytic activity.

The electrocatalytic activity of **MPc-CP**s for ORR was initially evaluated by CV in O_2-saturated and O_2-free electrolyte in 0.1 M KOH solution on **MPc-CP**-loaded glassy carbon electrodes with 50 wt% carbon black (Vulcan XC-72) to increase the electrical conductivity. As seen in Fig. 2a, for O_2-free electrolyte, the current in the CV curves showed featureless slopes for the cathodic current within the entire potential range. In contrast, the well-defined cathodic peaks at 0.7-0.9 V appeared in the CV curves of all the three **MPc-CP**s in O_2-saturated electrolyte, indicating their ORR catalytic activity. In particular, the peak potential positively shifted from 0.72 V for **CoPc-CP** and 0.80 V for **FePc-CP** to 0.86 V for **$Fe_{0.5}Co_{0.5}$Pc-CP**, revealing the significantly enhanced ORR catalytic activity of the heterometallic material. Linear sweep voltammetry (LSV) curves were recorded in O_2-saturated 0.1 M KOH solution to further investigate their ORR activity. In order to clarify the factors contributing to the ORR performance of the **MPc-CP**s glassy carbon electrode, the electrocatalysis properties of pure XC-72 and **MPc-CP**&XC-72 mixtures with different contents were measured as the reference (Fig. S9-S11 in ESI†). For the purpose of comparison, the ORR activity of the commercial Pt/C (20 wt%) as well as corresponding Pc-monomers were also studied, Fig. 2b and S12 (ESI†). As can be seen in Fig. S9 (ESI†), the ORR activity of **$Fe_{0.5}Co_{0.5}$Pc-CP**&XC-72 mixtures is significantly superior to that of pure XC-72 and **$Fe_{0.5}Co_{0.5}$Pc-CP** electrodes. The mixture with 50 wt% **$Fe_{0.5}Co_{0.5}$Pc-CP** exhibits the best catalytic behavior. The same cases for the **FePc-CP**-loaded and **CoPc-CP**-loaded electrodes as shown in Fig. S10 and S11 (ESI†). These results demonstrate that the ORR activity of the **MPc-CP**-loaded electrodes mainly originates from the synergistic effect between the highly active catalytic centers of **MPc-CP**s materials and high electrical conductivity of XC-72. In addition, it is worth noting that highly conjugated structures of these phthalocyanine-based CPs are beneficial to improve the interaction between phthalocyanine-based CPs and XC-72, which increases the electron-transfer efficiency during the electrocatalytic process and in turn improves the ORR performance.

Fig. 2b compares the LSV curves of **MPc-CP**s mixed with 50 wt% XC-72 and the commercial Pt/C (20 wt%) in O_2-saturated 0.1 M KOH solution at a scan rate of 10 mV·s^{-1} with the rotation speed of 1600 rpm. In good agreement with the CV study result, **$Fe_{0.5}Co_{0.5}$Pc-CP** displays the highest activity among the three Pc polymers in terms of onset potential (E_{onset}), the half-wave potential ($E_{1/2}$), and limiting current density (J_L). As shown in Fig. 2c and Table S1 (ESI†), **$Fe_{0.5}Co_{0.5}$Pc-CP** exhibits an E_{onset} of 937 mV and an $E_{1/2}$ of 848 mV with a J_L of -5.98 mA cm^{-2}. These results are significantly

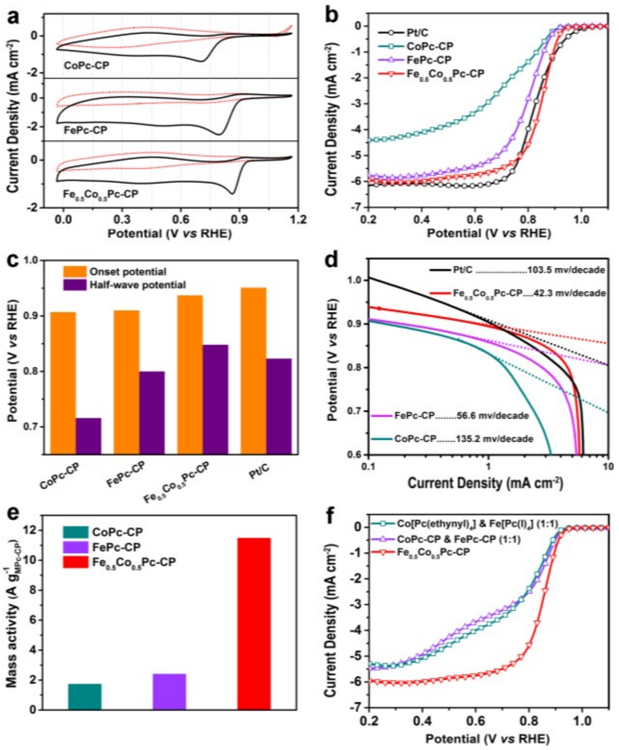

Fig. 2 (a) CVs of **MPc-CP**s in O_2-saturated (solid line) and O_2-free (dotted line) 0.1 M KOH solution. (b) LSV curves of **MPc-CP**s as well as the commercial Pt/C (20%) measured at the scan rate of 10 mV s^{-1} with the rotation speed of 1600 rpm in O_2-saturated 0.1 M KOH solution. (c) Half-wave potential and onset potential comparisons of the synthesized **MPc-CP**s as well as the commercial Pt/C (20%). (d) Tafel plots derived from the corresponding 1600 rpm LSV curves of the synthesized **MPc-CP**s as well as the commercial Pt/C (20%). (e) Comparison of the mass activity for **MPc-CP**s at 0.9 V (*vs* RHE). (f) LSV curves of Co[Pc(ethynyl)$_4$] & Fe[Pc(I)$_4$] (1:1), **CoPc-CP** & **FePc-CP** (1:1), and **Fe$_{0.5}$Co$_{0.5}$Pc-CP** in O_2-saturated 0.1 M KOH solution. All the data for the synthesized **MPc-CP**s were measured by doping with 50 wt% XC-72.

superior to the homometallic counterparts **FePc-CP** (E_{onset} = 910 mV, $E_{1/2}$ = 800 mV, and J_{L}= -5.76 mA cm^{-2}) and **CoPc-CP** (E_{onset} = 907 mV, $E_{1/2}$ = 716 mV, and J_{L} = -4.40 mA cm^{-2}), and are comparable to the commercially available Pt/C catalyst (E_{onset} = 951 mV, $E_{1/2}$ = 823 mV, and J_{L} = -6.14 mA cm^{-2}). Moreover, the superior ORR kinetics of the heterometallic compound to the homometallic counterparts was also clearly revealed by the significantly smaller Tafel slope of 42.3 mV dec^{-1} for **Fe$_{0.5}$Co$_{0.5}$Pc-CP** at low overpotentials than 56.6 and 135.2 mV dec^{-1} for **FePc-CP** and **CoPc-CP**, respectively (Fig. 2d). The electrochemical active surface areas (ECSAs) of the three **MPc-CP**s were also calculated in 0.1 M KOH solution by the reported method.[18] The ECSAs of the three **MPc-CP**s are similar under the same catalyst loading owing to their similar polymer network structures (Fig. S13 in ESI†). The mass activities of the three **MPc-CP**s were calculated to further assess their performance. As shown in Fig. 2e, the **Fe$_{0.5}$Co$_{0.5}$Pc-CP** shows mass activity of 11.5 A/g$_{\text{MPc-CP}}$ at 0.9 V vs RHE, which is about 5 and 7 times higher than those of **FePc-CP** (2.42 A/g$_{\text{MPc-CP}}$) and **CoPc-CP** (1.76 A/g$_{\text{MPc-CP}}$), respectively. The activity is also comparable to the best values reported for non-precious metal based electrocatalysts.[16c,19] These results suggest the synergetic effect between Fe and Co ions in **Fe$_{0.5}$Co$_{0.5}$Pc-CP** on promoting the ORR. In order to further verify this assumption, polarization curves of the corresponding Pc monomers for the three Pc polymers **MPc-CP**s were also recorded under the same testing conditions. As can be seen in Fig. S12 (ESI†), the compared results clearly indicate the only slightly increased ORR catalytic activity of **FePc-CP** and **CoPc-CP** over their Pc monomers. However, **Fe$_{0.5}$Co$_{0.5}$Pc-CP** shows significantly more positive E_{onset} and $E_{1/2}$ as well as the greater J_{L} than those of corresponding Pc-monomer electrode under the same loading amount (Fig. 2f). Moreover, **Fe$_{0.5}$Co$_{0.5}$Pc-CP** displays better catalytic activity over the mixture of **FePc-CP** and **CoPc-CP** (1:1) as seen in Fig. 2f, indicating that the improved ORR catalytic activity of **Fe$_{0.5}$Co$_{0.5}$Pc-CP** is due to the ordered distribution of Fe and Co center in the close proximity.

In order to gain further insight into the ORR catalytic activity, LSV curves on the **MPc-CP**-loaded electrodes with 50 wt% black carbon were recorded at the rotation speed range of 400-2500 rpm as seen in Fig. 3a, S14, and S15 (ESI†). The Koutecky-Levich (K-L) plots of all the **MPc-CP**-loaded

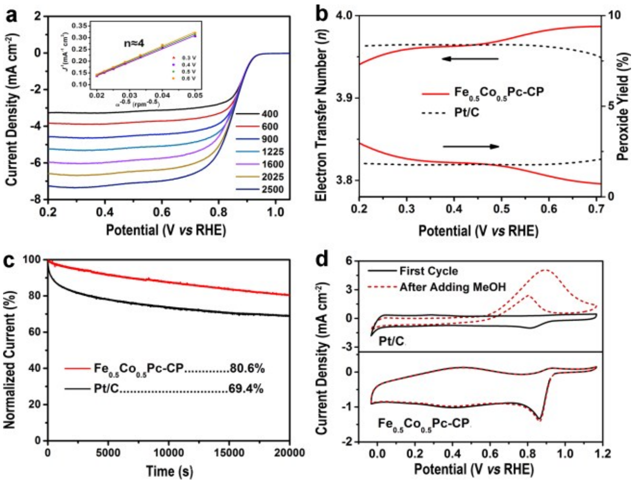

Fig. 3 (a) LSV curves of **Fe$_{0.5}$Co$_{0.5}$Pc-CP** at different rotation speeds. Insert: Koutecky–Levich (K–L) plots at different potentials. (b) Percentage of peroxide species and the electron-transfer number (*n*) of **Fe$_{0.5}$Co$_{0.5}$Pc-CP** and the commercial Pt/C (20%) in the potential range of 0.20-0.70 V (calculated from the corresponding RRDE data). (c) Amperometric i–t curves of **Fe$_{0.5}$Co$_{0.5}$Pc-CP** and the commercial Pt/C-modified electrode tested with the rotation speed of 1600 rpm in O_2-saturated 0.1 M KOH solution. (d) Methanol tolerance test with 5% methanol (in volume) in O_2-saturated 0.1 M KOH solution for **Fe$_{0.5}$Co$_{0.5}$Pc-CP** and Pt/C (20%) (the CV scan rate is 50 mV s^{-1}). All the data for the synthesized **MPc-CP**s were measured by doping with 50 wt% XC-72.

View Article Online
DOI: 10.1039/C8TA00516H

electrodes under different potentials exhibit good linearity and parallelism, indicating the first-order reaction kinetics toward the concentration of dissolved O_2. The *n* for both **$Fe_{0.5}Co_{0.5}$Pc-CP** and **FePc-CP** was calculated to be *ca*. 4 at 0.3-0.6 V, indicating the ORR at these electrodes proceeds by a $4e^-$ reduction pathway, similar to the commercial Pt/C electrode. In contrast, the *n* derived from the K-L plots for **CoPc-CP** is 3.6 ± 0.1 at 0.3-0.6 V, suggesting the co-existence of $2e^-$ and $4e^-$ oxygen reduction processes in this electrode. This is further supported by the rotation ring-disk electrode (RRDE) test with *n* calculated to be over 3.9 and low peroxide yield for the two Fe-containing electrodes, **$Fe_{0.5}Co_{0.5}$Pc-CP** and **FePc-CP**, in comparison with the values of *ca.* 3.5 and 20% for **CoPc-CP** at 0.2-0.7 V (Fig. 3b and S16 in ESI†). These results indicate preferential $2e^-$-reduction in **CoPc-CP** with respect to FePc-containing catalysts, in line with previous findings on catalytic selectivity in MPc-based catalysts.[11] Besides, the near four-electron pathway toward oxygen reduction on **$Fe_{0.5}Co_{0.5}$Pc-CP**-loaded electrode further reflects the high ORR efficiency of the heterometallic catalyst. Besides the high ORR activity, the long-term stability and possible fuel crossover effect are also quite important. Thus, the durability of the **$Fe_{0.5}Co_{0.5}$Pc-CP** with 50 wt% XC-72 and commercial Pt/C is evaluated through chronoamperometric measurements. As shown in Fig. 3c, **$Fe_{0.5}Co_{0.5}$Pc-CP** exhibits a superior long-term stability to the commercial Pt/C catalyst. The almost same XPS spectra of **$Fe_{0.5}Co_{0.5}$Pc-CP** before and after i-t test further confirm its high stability (see Fig. S17 in ESI†). We believe that the polymerization of $Fe[Pc(I)_4]$ and $Co[Pc(ethynyl)_4]$ into **$Fe_{0.5}Co_{0.5}$Pc-CP**, which could significantly improve the physical and chemical robustness, contributes to such high stability.[16a,c] In addition, after the durability test for 20000 s, the **FePc-CP** and **CoPc-CP** could retain around 70.1% and 77.2% of the initial current, respectively, compared to 80.6% for **$Fe_{0.5}Co_{0.5}$Pc-CP**, (see Fig. S18 in ESI†), suggesting the synergetic effect between Fe and Co ions may also be responsible for the high stability of **$Fe_{0.5}Co_{0.5}$Pc-CP**. Moreover, **$Fe_{0.5}Co_{0.5}$Pc-CP** was almost free from the methanol crossover effect, Fig. 3d. These results render **$Fe_{0.5}Co_{0.5}$Pc-CP** a promising candidate to replace the cathodic Pt/C catalyst in methanol fuel cells.

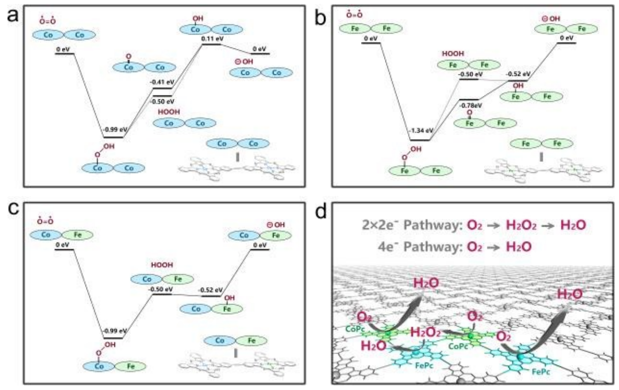

Fig. 4 Free-energy diagram of the ORR on (a) CoPc≡CoPc, (b) FePc≡FePc, and (c) FePc≡CoPc models at 1.23 V *vs.* RHE in alkaline media. d) Proposed ORR reaction mechanism at the **$Fe_{0.5}Co_{0.5}$Pc-CP** electrode.

DFT calculations.

Based on experimental results aforementioned, the higher catalytic activity of the heterometallic conjugated network **$Fe_{0.5}Co_{0.5}$Pc-CP** originates from the synergistic effect between the proximate Fe and Co ions. In an attempt to understand the synergetic effect, density functional theory (DFT) calculations were carried out at the level of PBE1PBE-GD3//SDD/6-311++G(2d,p)/6-311G(d).[20] Three computational models including FePc≡FePc, CoPc≡CoPc, and FePc≡CoPc, were derived from the basic structural units of the three **MPc-CP**s. As expected, the metal ions act as the active sites for ORR in all the three models. For the homometallic models, the $4e^-$ oxygen reduction reaction proceeds along the following pathways (* = surface):

$$O_2 + * + H_2O + e^- \rightarrow OOH* + OH^- \qquad (1)$$

$$OOH* + e^- \rightarrow O* + OH^- \qquad (2)$$

$$O* + H_2O + e^- \rightarrow OH* + OH^- \qquad (3)$$

$$OH* + e^- \rightarrow OH^- + * \qquad (4)$$

When the reaction proceeds along the following path 2' rather than 2 after step 1, H_2O_2 is generated by a $2e^-$ oxygen reduction:

$$OOH* + H_2O + e^- \rightarrow H_2O_2* + OH^- \qquad (2')$$

Fig. 4 shows the calculated free-energy diagrams of all the ORR intermediates involved in steps 1-4 and 2' bound on the active site at 1.23 V *vs.* RHE. In the FePc≡FePc model, the activation barrier of step 2 is lower than that for 2' (H_2O_2 generation reaction). As a consequence, the ORR reaction prefers to proceed following the $4e^-$ route in the FePc≡FePc network of **FePc-CP**. It is suggested that uphill process of step 2 with activation barrier of 0.56 eV is the overall rate-limiting step. For the CoPc≡CoPc model, step 2 is also the rate-limiting step for the $4e^-$ route with activation barrier of 0.58 eV, similar to the FePc≡FePc model. However, the activation barrier of step 2 is higher than that of step 2' in the CoPc≡CoPc model, then the $2e^-$ reduction pathway is more favorable with the generation of a significant amount of H_2O_2 in this model. It is worth noting that after step 2', H_2O_2 generated then could be reduced into OH^- following steps 3' and 4.

$$H_2O_2 + e^- + * \rightarrow OH* + OH^- \qquad (3')$$

However, owing to the higher activation barrier of 0.61 eV for step 3' in the CoPc≡CoPc model as shown in Fig. 4a, the further reduction of H_2O_2 could proceed only at low potential. In addition, the significant amount of H_2O_2 generated around the Co centers in turn limit the further adsorption and reduction of O_2 on these Co centers, resulting in the slow ORR kinetics as a whole in the CoPc≡CoPc network of **CoPc-CP**. This corresponds well with the experimental findings that **CoPc-CP** displays similar E_{onset} but significantly larger Tafel slope and smaller $E_{1/2}$ in comparison with **FePc-CP** (Fig. 2b and 2d). In the case of the heterometallic model FePc≡CoPc, the reaction free energy for the reduction of O_2 to H_2O_2 at the Co center *via* steps 1 and 2', 0.49 eV, is obviously smaller than that of the reactions through steps 1-2, 0.56 eV, at the Fe center, inducing O_2 is preferred to be adsorbed at the Co center with H_2O_2 as the resulting intermediate at this stage. Nevertheless, Fe center possesses higher peroxide reduction reaction catalytic activity through the steps 3′ and 4 than Co center as revealed by the obviously lower activation barrier for the former process, 0.52 eV, than for the latter, 0.61 eV. Continuous reaction then moves from the Co center to the Fe to complete the whole ORR process. As a total result, oxygen reduction in the heterometallic FePc≡CoPc model actually proceeds through steps 1, 2′ at the Co center by a $2e^-$ reduction pathway *via* peroxide generation, and then through steps 3′ and 4 at Fe center by another $2e^-$ reduction pathway *via* peroxide reduction with the activation barrier of 0.52 eV, smaller than those of both homometallic models (Fig. 4). Such a fast $2 \times 2e^-$ synergetic catalytic reaction pathway results in the superior ORR electrochemical catalytic activity for $Fe_{0.5}Co_{0.5}$Pc-CP to both homometallic analogues.

To support the calculation result, the electrochemical activity of the **MPc-CP**s for H_2O_2 reduction was investigated by means of the chronoamperometry method. Fig. S19 in ESI† exhibits the response curve of steady-state i–t for the **MPc-CP**s modified electrode to the successive addition of 1 mM H_2O_2 into N_2-saturated 0.1 M KOH solution in the potential range of 570 and 930 mV (*vs*. RHE). As can be seen, the sharp step of current reduction following the addition of H_2O_2 could be observed for **$Fe_{0.5}Co_{0.5}$Pc-CP**, **FePc-CP**, and **CoPc-CP** under the applied potential below 930, 930, and 870 mV, respectively. The polymer containing Fe shows higher activity, revealing the effect of the Fe center towards H_2O_2 reduction. These results support the calculation data in which the polymers with Fe centers are promoting H_2O_2 reduction (step 3′ and 4). Combined with H_2O_2 regeneration promoted by the Co centers, it is supported that **$Fe_{0.5}Co_{0.5}$Pc-CP** exhibits the $2 \times 2e^-$ synergetic catalytic reaction pathway, as indicated by the DFT calculations. In addition, the $2 \times 2e^-$ synergetic catalytic reaction pathway in **$Fe_{0.5}Co_{0.5}$Pc-CP** involves the transfer of peroxide from Co centers to Fe centers. As a consequence, the Fe and Co ions synergistic effect might get weakened along with increasing the distance between the Fe and Co ions and therefore result in lower ORR performance. In order to verify this assumption, a conjugated diyne (−C≡C−C≡C−) linked heterometallic Pc conjugated polymer **$Fe_{0.5}Co_{0.5}$Pc-CP-2** was synthesized by the alkyne–alkyne homocoupling reaction between Fe[Pc(ethynyl)$_4$] and Co[Pc(ethynyl)$_4$] with larger distance between the Fe and Co than that in the −C≡C− linked **$Fe_{0.5}Co_{0.5}$Pc-CP**. **$Fe_{0.5}Co_{0.5}$Pc-CP-2** exhibits an E_{onset} of 912 mV and an $E_{1/2}$ of 817 mV, Fig. S20 in ESI†. Both are similar to those of **FePc-CP** (E_{onset} = 910 mV and $E_{1/2}$ = 800 mV) but smaller than those of **$Fe_{0.5}Co_{0.5}$Pc-CP** (E_{onset} = 937 mV and $E_{1/2}$ = 848 mV). These results suggest that **$Fe_{0.5}Co_{0.5}$Pc-CP-2** is very likely to be an Fe conjugated polymer itself, without the synergistic effect of Fe and Co, revealing the effect of the distance between the Fe and Co ions on the their synergistic effect.

Conclusions

We have successfully prepared an ethynyl-linked Fe/Co heterometallic Pc-based 2D conjugated polymer **$Fe_{0.5}Co_{0.5}$Pc-CP** with alternate distribution of Fe and Co fragments by rational design and artful synthesis. The derived heterometallic polymer exhibits superior ORR catalytic activity to the homometallic counterparts, which is comparable to the commercially available Pt/C catalyst. Based on the experimental analysis and DFT calculations, the excellent ORR catalytic activity of **$Fe_{0.5}Co_{0.5}$Pc-CP** is attributed to the synergetic effect between the proximate Fe and Co ions in the conjugated network, which results in a fast $2 \times 2e^-$ synergetic catalytic reaction pathway. This work is not only helpful for gaining insight into the origin of the ORR catalytic activity for $FeCoN_x$-based catalysts, but also offers a practical way to develop novel electrocatalysts with well-defined chemical composition and structure for various electrochemical reactions.

Experimental Section

General Remarks

THF and Et_3N were distilled from Na and CaH_2, respectively. All other reagents and solvents were reagent grade and used as received. The compounds Fe[Pc(I)$_4$],[12] Fe[Pc(ethynyl)$_4$],[12] Co[Pc(I)$_4$],[12] and Co[Pc(ethynyl)$_4$][12] were prepared according to methods in literatures. All coupling reactions were carried out under a nitrogen atmosphere.

The ^{13}C CP/TOSS NMR spectra were recorded with a 4-mm MAS probe and with a sample spinning rate of 3.0 kHz. IR spectra were recorded as KBr pellets using a Bruker Tensor 37 spectrometer with 2 cm^{-1} resolution. Powder X-ray diffraction (PXRD) data were collected on a Shimadzu XRD-6000 diffractometer using Cu-Kα radiation (I = 1.54056 Å) at room temperature. SEM images were obtained using a JEOL JEM-6510A scanning electron microscopy. The morphology and mapping of the catalysts were investigated by transmission electron microscopy (TEM, JEM-2100F, JEOL, Japan) at an operation voltage of 200 kV. The Fe and Co contents of the **MPc-CP**s were determined by inductively coupled plasma atomic emission spectroscopy (ICP-AES) analysis with an IRIS Intrepid II XRP instrument. XPS was carried out on PHI 5300 ESCA System (PerkineElmer, USA). Solid-state UV-Vis diffuse reflectance spectra were recorded on an SHIMADZU UV-2600 spectrophotometer. The excitation source is Al Kα radiation. TGA was performed on a PerkinElmer TG-7 analyzer with a heating rate of 10 °C min^{-1} in the range of 25-900 °C under N_2 atmosphere. CV, LSV, and RRDE measurements were conducted on the CHI 760E workstation (CH Instruments, Inc.) with a RRDE-3A rotator (ALS Co., Ltd). The typical three-electrode system was employed to evaluate the electrochemical properties of the prepared catalysts. Specifically, glassy carbon was the working electrode, a Pt wire was the counter electrode, and the Ag/AgCl (in saturated KCl solution) was the reference electrode. All potentials were referred to the reversible hydrogen electrode by adding a value of (0.197 + 0.059×pH) V. All the electrochemical tests in

View Article Online
DOI: 10.1039/C8TA00516H

this study were conducted at least three times to ensure the accuracy of the measurement. Besides, the iR correction was applied to get rid of the influence of the Ohmic resistance, and the effect of the doublelayer capacitance on the ORR performance of the resulting catalysts was eliminated (the corresponding methods were specified below).

Synthesis of $Fe_{0.5}Co_{0.5}$Pc-CP

A mixture of Fe[Pc(I)$_4$] (128 mg, 0.12 mmol) and Co[Pc(ethynyl)$_4$] (80 mg, 0.12 mmol) in a mixture solvent of Et_3N (20 ml) and THF (10 ml) with the presence of catalysts $Pd(PPh_3)_2Cl_2$ (2.8 mg, 14.7 μmol) and CuI (0.8 mg, 4.2 μmol) was heated to 70°C for 48 h under N_2 atmosphere. After the mixture was cooled to room temperature, the precipitate was filtered and washed with THF, toluene, and methanol to remove any phthalocyanine monomers and catalysts. The product was dried at 80°C under vacuum for 12 h to yield **$Fe_{0.5}Co_{0.5}$Pc-CP** as a dark blue powder (190 mg, yield 92%). The Fe and Co content were 3.24% and 3.82% as determined by ICP-AES, respectively.

Synthesis of CoPc-CP

By employing the above-mentioned synthesis procedure of **$Fe_{0.5}Co_{0.5}$Pc-CP** with Co[Pc(I)$_4$] instead of Fe[Pc(I)$_4$] as starting material, **CoPc-CP** was isolated in the yield of 93%. The Co content was 7.14% as determined by ICP-AES.

Synthesis of FePc-CP

By employing the above-mentioned synthesis procedure of **$Fe_{0.5}Co_{0.5}$Pc-CP** with Fe[Pc(ethynyl)$_4$] instead of Co[Pc(ethynyl)$_4$] as starting material, **FePc-CP** was isolated in the yield of 95%. The Fe content was 6.89% as determined by ICP-AES.

Synthesis of $Fe_{0.5}Co_{0.5}$Pc-CP-2

A mixture of Fe[Pc(ethynyl)$_4$] (80 mg, 0.12 mmol) and Co[Pc(ethynyl)$_4$] (80 mg, 0.12 mmol) in a mixed solvent of Et_3N (20 ml) and THF (10 ml) in the presence of catalysts $Pd(PPh_3)_2Cl_2$ (2.8 mg, 14.7 μmol) and CuI (0.8 mg, 4.2 μmol) was heated to 70°C for 48 h under N_2 atmosphere. After the mixture was cooled to room temperature, the precipitate was filtered and washed with THF, toluene, and methanol to remove any phthalocyanine monomers and catalysts. The product was dried at 80°C under vacuum for 12 h to yield **$Fe_{0.5}Co_{0.5}$Pc-CP-2** as a dark blue powder (156 mg, yield 98%).

Preparation of the working electrode

The catalyst ink was prepared by dispersing 4 mg of sample into 1.5 mL ethanol and 0.5 mL deionized water solvent containing 0.5 μL 5wt% Nafion and sonicated for 60 min. Then, 10 μL of the mixture was dropped onto a polished glassy carbon electrode (4 mm in diameter). The loaded electrode was placed in a 60 °C oven for 10 min to dry and then was taken out to cool down before all the tests. The corresponding catalyst loading is 0.08 mg cm^{-2}

Cyclic voltammetry (CV).

Prior to the test, the electrolyte (0.1 M KOH solution) was bubbled with O_2 for at least 30 min to make it saturated with O_2, and a constant oxygen flow was kept during the measurement. The data was recorded at the scan rate of 50 mV s^{-1} under static conditions when the system became stable. For the methanol tolerance test, after injecting 5 % (volume) methanol into the cell, the electrode was rotated for 5 min to ensure the added methanol dispersed homogeneously in the electrolyte, and then the CV measurement was carried out under static conditions again. The resulting data were corrected to remove the iR drop.

Linear sweep voltammetry (LSV) measurement

The rotating speed of the working electrode is increased from 400 to 2500 rpm at the scan rate of 10 mV s^{-1}. The resulting data were corrected to remove the iR drop and the double-layer effect.

Rotating ring-disk electrode (RRDE) measurement

The rotating speed of the working electrode was fixed at 1600 rpm with the scan rate of 10 mV s^{-1} for the RRDE test. The electron transfer number (*n*) is calculated *via* the following equation.[4b]

$$n = 4I_d / (I_d + I_r / N)$$

$$\% \, HO^{2-} = 200(I_r / N) / (I_d + I_r / N)$$

Where I_d stands for the disk current, I_r represents the ring current, and N is the current collection efficiency of the Pt ring, which was identified to be 0.43 in 2 mmol L^{-1} $K_3Fe[CN]_6$ and 0.1 M KCl solution.

Koutecky-Levich (K-L) plots

The working electrode was scanned cathodically at the rate of 10 mV s^{-1} with the rotation speed from 400 to 2500 rpm. Koutecky-Levich (K-L) plots (J^{-1} *vs* $\omega^{-1/2}$) were analyzed at 0.3-0.6 V. Koutecky-Levich equation: [21]

$$1/J = 1/J_L + 1/J_K = 1/(B\omega^{1/2}) + 1/J_K$$

$$B = 0.2nFC_0D_0^{2/3}v^{-1/6}; \; J_K = nFkC_0$$

Where J is the measured current density, J_k and J_L are the kinetic and limiting current densities, ω is the angular velocity, n is transferred electron number, F (96485 C mol^{-1}) is the Faraday constant, D_0 is the diffusion coefficient of O_2 in 0.1 M KOH (1.9 × 10^{-5} cm^2 s^{-1}), C_0 is the bulk concentration of O_2 (1.2 × 10^{-6} mol cm^{-3}), v is the kinetic viscosity of the electrolyte (0.01 cm^2 s^{-1}), and k is the electron-transfer rate constant. The constant 0.2 is adopted when the rotation speed is expressed in rpm.

iR-Correction

The iR correction has been adopted to remove the influence of Ohmic resistance on the ORR measurements. Specifically, the electrochemical alternating current impedance spectroscopy (EIS) was utilized to measure to Ohmic resistance under the ORR conditions. The potentials were calculated *via* the following equation:[22]

$$E_{\text{iR-corrected}} = E - iR$$

Where i is the current, R is the uncompensated ohmic electrolyte resistance measured *via* high frequency A.C.

impedance in O_2-saturated 0.1 M KOH solution, which is around 50 Ω for all the tested samples.

Double-Layer Capacitance Correction

The ORR test was conducted in ultra-high purity nitrogen saturated and oxygen saturated 0.1 M KOH solution, respectively, and the final LSV data was obtained by subtracting the LSV data measured in N_2-saturated 0.1 M KOH solution from the LSV results measured in O_2-saturated 0.1 M KOH solution. All the LSV curves in this work have been corrected by this method.

Mass Activity

The mass activity was obtained by normalizing the kinetic current (I_k) to the electrode mass. I_k is obtained by multiplying J_k (derived from the Koutecky-Levich equation at 0.9 V *vs* RHE) with the geometric area of the glassy carbon disk.

Theoretical Calculation

Density functional theory (DFT) calculations were carried out using PBE1PBE-GD3.[20] A mixed basis set, including SDD[23] for Fe/Co and 6-311++G(2d,p)/6-311G(d)[24] for C\H\N\O, was employed. All the Gibbs free energy values were calculated using the Nørskov model.[25]

Acknowledgements

Financial support from the Natural Science Foundation of China (Nos. 21631003, 21671017, 21290174, and 21401009), the National Key Basic Research Program of China (Grant No. 2013CB933402), and China Scholarship Council. University of Science and Technology Beijing is gratefully acknowledged.

References

1 (a) B. C. H. Steele and A. Heinzel, *Nature,* 2001, **414**, 345-352; (b) E. M. Erickson, M. S. Thorum, R. Vasic, N. S. Marinkovic, A. I. Frenkel, A. A. Gewirth and R. G. Nuzzo, *J. Am. Chem. Soc.,* 2012, **134**, 197-200.

2 (a) C. Chen, Y. Kang, Z. Huo, Z. Zhu, W. Huang, H. L. Xin, J. D. Snyder, D. Li, J. A. Herron, M. Mavrikakis, M. Chi, K. L. More, Y. Li, N. M. Markovic, G. A. Somorjai, P. Yang and V. R. Stamenkovic, *Science,* 2014, **343**, 1339-1343; (b) Y.-J. Wang, B. Fang, X. T. Bi, Y.-J. Wang, N. Zhao, H. Li and H. Wang, *Chem Rev.,* 2015, **115**, 3433-3467.

3 (a) B. Y. Xia, Y. Yan, N. Li, H. B. Wu, X. W. Lou and X. Wang, *Nat. Energy,* 2016, **1**, 15006; (b) J. C. Meier, I. Katsounaros, C. Galeano, H. J. Bongard, A. A. Topalov, A. Kostka, A. Karschin, F. Schueth and K. J. J. Mayrhofer, *Energy Environ. Sci.,* 2012, **5**, 9319-9330.

4 (a) Z. Chen, D. Higgins, A. Yu, L. Zhang and J. Zhang, *Energy Environ. Sci.,* 2011, **4**, 3167-3192; (b) Y. Liang, Y. Li, H. Wang, J. Zhou, J. Wang, T. Regier and H. Dai, *Nat. Mater.,* 2011, **10**, 780-786; (c) Y. Tong, P. Chen, T. Zhou, K. Xu, W. Chu, C. Wu and Y. Xie, *Angew. Chem., Int. Ed.,* 2017, **56**, 7121-7125; (d) X. Yan, Y. Jia, J. Chen, Z. Zhu and X. Yao, *Adv. Mater.,* 2016, **28**, 8771-8778.

5 (a) D. Guo, T. Kondo, J. Nakamura, R. Shibuya, C. Akiba and S. Saji, *Science*, 2016, **351**, 361-365; (b) L. Dai, Y. Xue, L. Qu, H.-J. Choi and J.-B. Baek, *Chem. Rev.*, 2015, **115**, 4823-4892; (c) J. Zhang, L. Qu, G. Shi, J. Liu, J. Chen and L. Dai, *Angew. Chem., Int. Ed.*, 2016, **55**, 2230-2234; (d) Y. Jia, L. Zhang, A. Du, G. Gao, J. Chen, X. Yan, C. L. Brown and X. Yao, *Adv. Mater.*, 2016, **28**, 9532-9538.

6 (a) X. Yan, Y. Jia, J. Chen, Z. Zhu and X. Yao, *Adv. Mater.*, 2016, **28**, 8771-8778; (b) P. Yin, T. Yao, Y. Wu, L. Zheng, Y. Lin, W. Liu, H. Ju, J. Zhu, X. Hong, Z. Deng, G. Zhou, S. Wei and Y. Li, *Angew. Chem., Int. Ed.*, 2016, **55**, 10800-10805; (c) P. Chen, T. Zhou, L. Xing, K. Xu, Y. Tong, H. Xie, L. Zhang, W. Yan, W. Chu, C. Wu and Y. Xie, *Angew. Chem., Int. Ed.*, 2017, **56**, 610-614; (d) H. Zhang, S. Hwang, M. Wang, Z. Feng, S. Karakalos, L. Luo, Z. Qiao, X. Xie, C. Wang, D. Su, Y. Shao and G. Wu, *J. Am. Chem. Soc.*, 2017, **139**, 14143-14149.

7 (a) A. Zitolo, N. Ranjbar-Sahraie, T. Mineva, J. Li, Q. Jia, S. Stamatin, G. F. Harrington, S. M. Lyth, P. Krtil, S. Mukerjee, E. Fonda and F. Jaouen, *Nature Commun.*, 2017, **8**, 957; (b) Q. Jia, N. Ramaswamy, U. Tylus, K. Strickland, J. Li, A. Serov, K. Artyushkova, P. Atanassov, J. Anibal, C. Gumeci, S. C. Barton, M.-T. Sougrati, F. Jaouen, B. Halevi and S. Mukerjee, *Nano Energy*, 2016, **29**, 65-82; (c) J. Li, S. Ghoshal, W. Liang, M.-T. Sougrati, F. Jaouen, B. Halevi, S. McKinney, G. McCool, C. Ma, X. Yuan, Z.-F. Ma, S. Mukerjee and Q. Jia, *Energy Environ. Sci.*, 2016, **9**, 2418-2432; (d) U. I. Kramm, I. Herrmann-Geppert, S. Fiechter, G. Zehl, I. Zizak, I. Dorbandt, D. Schmeißer and P. Bogdanoff, *J. Mater. Chem. A*, 2014, **2**, 2663-2670.

8 (a) Q. Lin, X. Bu, A. Kong, C. Mao, F. Bu and P. Feng, *Adv. Mater.*, 2015, **27**, 3431-3436; (b) G. Wu, K. L. More, C. M. Johnston and P. Zelenay, *Science*, 2011, **332**, 443-447; (c) J. Wang, Z. Huang, W. Liu, C. Chang, H. Tang, Z. Li, W. Chen, C. Jia, T. Yao, S. Wei, Y. Wu and Y. Li, *J. Am. Chem. Soc.*, 2017, **139**, 17281-17284; (d) Y. Zhao, K. Watanabe and K. Hashimoto, *J. Mater. Chem. A*, 2013, **1**, 1450-1456.

9 (a) Y. Xu, S. Jin, H. Xu, A. Nagai and D. Jiang, *Chem. Soc. Rev.*, 2013, **42**, 8012-8031; (b) Z. Xiang and D. Cao, *J. Mater. Chem. A*, 2013, **1**, 2691-2718; (c) F. Vilela, K. Zhang and M. Antonietti, *Energy Environ. Sci.*, 2012, **5**, 7819-7832; (d) K. Wang, D. Qi, Y. Li, T. Wang, H. Liu and J. Jiang, *Coord. Chem. Rev.*, 2017, DOI: 10.1016/j.ccr.2017.08.023.

10 R. Jasinski, *Nature*, 1964, **201**, 1212-1213.

11 (a) L. Cui, G. Lv and X. He, *J. Power Sources*, 2015, **282**, 9-18; (b) W. Zhang, W. Lai and R. Cao, *Chem. Rev.*, 2017, **117**, 3717−3797; (c) Y. Jiang, Y. Lu, X. Lv, D. Han, Q. Zhang and L. Niu, W. Chen, *ACS Catal.* 2013, **3**, 1263−1271; (d) L. Chen, Y. Yang and D. Jiang, *J. Am. Chem. Soc.*, 2010, **132**, 9138-9143; (e) J. H. Zagal and M. T. M. Kope, *Angew. Chem. Int. Ed.*, 2016, **55**, 14510-14521.

12 E. M. Maya, P. Haisch, P. Vazquez and T. Torres. *Tetrahedron*, 1998, **54**, 4397-4404.

13 J. Jiang, M. Bao, L. Rintoul and D. P. Arnold, *Coord. Chem. Rev.*, 2006, **250**, 424-448.

14 Z. Wang, S. Yuan, A. Mason, B. Reprogle, D. J. Liu and L. Yu, *Macromolecules*, 2012, **45**, 7413-7419.

15 L. Zhang, K. Wang, X. Qian, H. Liu and Z. Shi, *ACS Appl. Mater. Interfaces*, 2013, **5**, 2761−2727.

View Article Online
DOI: 10.1039/C8TA00516H

16 (a) H. Jia, Z. Sun, D. Jiang, S. Yang and P. Du, *Inorg. Chem. Front.*, 2016, **3**, 821-827; (b) M. E. Lipinska, J. P. Novais, S. L. H. Rebelo, B. Bachiller-Baeza, I. Rodriguez-Ramos, A. Guerrero-Ruiz and C. Freire, *Polyhedron*, 2014, **81**, 475-484; (c) X. Wang, B. Wang, J. Zhong, F. Zhao, N. Han, W. Huang, M. Zeng, J. Fan and Y. Li, *Nano Research*, 2016, **9**, 1497-1506.

17 (a) H. Tang, H. Yin, J. Wang, N. Yang, D. Wang and Z. Tang, *Angew. Chem. Int. Ed.*, 2013, **52**, 5585-5589; (b) J. Sun, H. Yin, P. Liu, Y. Wang, X. Yao, Z. Tang and H. Zhao, *Chem. Sci.*, 2016, **7**, 5640-5646.

18 H. Fei, J. Dong, M. J. Arellano-Jimenez, G. Ye, N. Dong Kim, E. L. G. Samuel, Z. Peng, Z. Zhu, F. Qin, J. Bao, M. J. Yacaman, P. M. Ajayan, D. Chen and J. M. Tour, *Nat. Commun.*, 2015, **6**, 8668.

19 (a) Y.-C. Wang, Y.-J. Lai, L. Song, Z.-Y. Zhou, J.-G. Liu, Q. Wang, X.-D. Yang, C. Chen, W. Shi and Y.-P. Zheng, *Angew. Chem., Int. Ed.*, 2015, **54**, 9907-9910; (b) K. P. Singh, E. J. Bae and J.-S. Yu, *J. Am. Chem. Soc.*, 2015, **137**, 3165–3168.

20 (a) C. Adamo and V. Barone, *J. Chem. Phys.*, 1999, **110**, 6158-6170; (b) M. Ernzerhof and G. E. Scuseria, *J. Chem. Phys.*, 1999, **110**, 5029-5036; (c) S. Grimme, J. Antony, S. Ehrlich and H. Krieg, *J. Chem. Phys.*, 2010, **132**, 154104-154119.

21 (a) Y. Liang, H. Wang, J. Zhou, Y. Li, J. Wang, T. Regier and H. Dai, *J. Am. Chem. Soc.*, 2012, **134**, 3517-3523; (b) S. Wang, D. Yu, L. Dai, D. W. Chang and J.-B. Baek, *ACS Nano*, 2011, **5**, 6202-6209.

22 Y. Zhu, W. Zhou, Z.-G. Chen, Y. Chen, C. Su, M. O. Tadé and Z. Shao, *Angew. Chem. Int. Ed.*, 2015, **54**, 3897-3901.

23 (a) A. Bergner, M. Dolg, W. Kuechle, H. Stoll and H. Preuss, *Mol. Phys.*, 1993, **80**, 1431-1441; (b) M. Kaupp, P. v. R. Schleyer, H. Stoll and H. Preuss, *J. Chem. Phys.*, 1991, **94**, 1360-1366; (c) M. Dolg, H. Stoll, H. Preuss and R. M. Pitzer, *J. Phys. Chem.*, 1993, **97**, 5852-5859.

24 R. Krishnan, J. S. Binkley, R. Seeger and J. A. Pople, *J. Chem. Phys.*, 1980, **72**, 650-654.

25 (a) J. K. Norskov, J. Rossmeisl, A. Logadottir, L. Lindqvist, J. R. Kitchin, T. Bligaard and H. Jonsson, *J. Phys. Chem. B*, 2004, **108**, 17886-17892; (b) H. A. Hansen, J. Rossmeisl and J. K. Norskov, *Phys. Chem. Chem. Phys.*, 2008, **10**, 3722-3730.

View Article Online
DOI: 10.1039/C8TA00516H

Ethynyl-linked Fe/Co Heterometallic Phthalocyanine Conjugated Polymer for Oxygen Reduction Reaction

Wenping Liu,[a] Yuxia Hou,[a,c] Houhe Pan,[a] Wenbo Liu,[a] Dongdong Qi,[a] Kang Wang,*[a,b] Jianzhuang Jiang*[a] and Xiangdong Yao[b]*

Heterometallic phthalocyanine 2D conjugated polymer with alternate distribution of Fe and Co fragments has been fabricated, exhibiting excellent oxygen reduction reaction catalytic activity comparable to Pt/C.